Fast compression of a cold atomic cloud using a blue-detuned crossed dipole trap

Tom Bienaimé,[*] Giovanni Barontini,[†] Laure Mercier de Lépinay, Louis Bellando, Julien Chabé, and Robin Kaiser
Université de Nice Sophia Antipolis, CNRS, Institut Non-Linéaire de Nice, UMR 7335, F-06560 Valbonne, France
(Received 4 July 2012; published 19 November 2012)

We present the experimental realization of a compressible blue-detuned crossed dipole trap for cold atoms allowing for fast dynamical compression (∼5–10 ms) of 5×10^7 rubidium atoms up to densities of $\sim 10^{13}$ cm^{-3}. The dipole trap consists of two intersecting tubes of blue-detuned laser light. These tubes are formed using a single, rapidly rotating laser beam which, for sufficiently fast rotation frequencies, can be accurately described by a quasistatic potential. The atomic cloud is compressed by dynamically reducing the trap volume, leading to densities close to the Ioffe-Regel criterion for light localization.

DOI: 10.1103/PhysRevA.86.053412 PACS number(s): 37.10.De, 37.10.Gh, 67.85.−d

I. INTRODUCTION

The use of optical dipole traps for manipulating and trapping ultracold atoms has been crucial to the evolution of this field of research. For example, they can be used to form a Bose-Einstein condensate (BEC) [1], create artificial crystals of light [2], or study physics in low dimensions by freezing the spatial degrees of freedom [3].

Light-matter interaction in the dense regime is a very dynamic and challenging field of research [4–6], where one of the long-standing problems is an understanding of the role of cooperative effects (superradiance [7,8], subradiance [9], collective Lamb shift [10]) and disorder (weak [11] and strong [12] localization). In order to reach this regime, a dipole trap can be used to compress the cloud to high densities where the strong-localization phase transition [12] is expected to occur at a threshold given by the Ioffe-Regel criterion [13] $kl \sim 1$, where $k = 2\pi/\lambda$ is the light wave vector and $l = 1/(n\sigma)$ is the mean free path (with n the atomic density and σ the scattering cross section). For resonant two-level systems, the scattering cross section $\sigma_0 = 3\lambda^2/(2\pi)$ allows the Ioffe-Regel criterion to be expressed as $n\lambda^3 \sim 1$. Such densities correspond for rubidium atoms to 10^{13}–10^{14} cm^{-3}, three orders of magnitude higher than magneto-optical-trap (MOT) densities. These high densities are commonly obtained in dipole traps for bosonic [1] or fermionic [14] ultracold gases. However, the relatively low number of atoms ($\sim 10^5$) and long duty cycles (∼10 s) make it difficult to efficiently study light-matter interaction in dense regimes [15] where a large number of atoms as well as short duty cycles are important assets for efficient detection of signatures of cooperative effects and/or strong localization of light. Indeed the Ioffe-Regel criterion should not be confused with the BEC threshold $n\Lambda_T^3 \sim 1$, where Λ_T is the thermal de Broglie wavelength. In contrast to Bose-Einstein condensation, we do not expect a drastic constraint on temperature for the Ioffe-Regel criterion of strong localization.

In this paper, we present a compressible blue-detuned crossed dipole trap to achieve a very fast dynamical compression (∼5–10 ms) of a large number of ^{87}Rb atoms ($\sim 5 \times 10^7$) to densities compatible with the Ioffe-Regel criterion, i.e., $\sim 10^{13}$ cm^{-3}. Trapping atoms in a "dark" region surrounded by blue-detuned light has several advantages, such as minimizing photon scattering, light shifts of the atomic levels, and light-assisted collisional losses [16]. Experimentally, blue-detuned trap are more difficult to produce than red ones. However, an original method [17] consists in using a focused Gaussian laser beam which is rapidly rotating and obtained by use of two perpendicular acousto-optical modulators (AOMs). If the rotation frequency is sufficiently high, the resulting time-averaged potential forms a tube of light. Crossing two of these tubes leads to a dark volume where atoms are trapped. This method allows dynamic control of the shape and the size of the trap which, for example, might be used to optimize the loading efficiency with a large trapping volume and then compress the cloud using a fast dynamical reduction of the trap size. These blue-detuned time-averaged potentials have been used in the past to study thermal cloud compression [17] and optical billiards and chaos [18–20], or to design microscopically tailored potentials for BECs [21] or ultracold Fermi gases [22]. For red dipole traps, a dynamical compression allowed quantum degeneracy to be reached via runaway evaporative cooling using a mobile lens to change the trap waist dynamically [23].

II. EXPERIMENTAL SETUP

A. Trap configuration

The trap consists of two tubes of blue-detuned light, crossed at 90° to create a box of light [see Fig. 1(a)] where the atoms are confined. The size and the shape of the box can be dynamically adjusted. Figure 1(b) shows the experimental setup used to create the tubes of light. A laser beam with 1 mm waist passes through two AOMs (Gooch & Housego M080-2B/F-GH2), crossed at 90°. The AOMs are powered by two radio-frequency (rf) signals whose instantaneous frequencies are respectively given by $f_1(t) = f_0 + \Delta f \cos(2\pi f_m t)$ and $f_2(t) = f_0 + \Delta f \sin(2\pi f_m t)$. The central frequency f_0 is fixed at 80 MHz, the modulation frequency amplitude Δf is at most 20 MHz and the modulation frequency f_m is generally set to 90 kHz. In the $(+1, +1)$ diffraction order of the AOMs, the laser beam is rotating at frequency f_m, and a lens, placed at a focal distance of 150 mm from the AOMs, creates a time-averaged tube of light with a diameter of 1 mm and a

[*]Present address: Niels Bohr Institute, University of Copenhagen, Blegdamsvej 17, DK-2100 Copenhagen, Denmark.
[†]Present address: Research Center OPTIMAS, Technische Universität Kaiserslautern, DE-67663 Kaiserslautern, Germany.

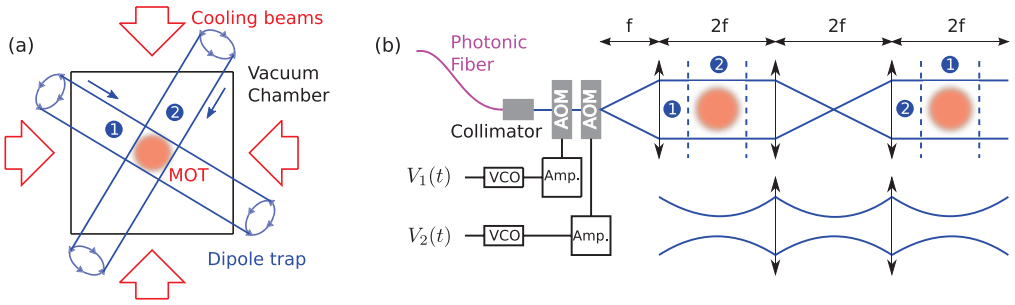

FIG. 1. (Color online) Sketch of the experimental setup. (a) Top view of the setup, showing the location of the two horizontal tubes forming the crossed blue-detuned dipole trap. (b) Details of the setup used to produce the two tubes [(+1, +1) orders of the AOMs]. On the top, only the contour of the trap is sketched while on the bottom only the beam profile is shown. For simplicity, we do not show the two mirrors that are used to cross the tubes 1 and 2 (the dashed lines show the position of the crossing). VCO indicates voltage-control oscillator.

waist of 65 μm in the lens focal plane where the atoms are trapped. Using a system of lenses and mirrors, the tube can be "recycled" and crossed at 90° from its initial direction (see Fig. 1). By varying the modulation frequency amplitude Δf, the trap size can be dynamically controlled.

A rotating laser beam with power P, waist w, and a radial intensity profile given by $I(x,y) = \frac{2P}{\pi w^2} \exp[-2(x^2+y^2)/w^2]$ describing a circle of radius a creates a time-average intensity profile

$$I(r) = \frac{2P}{\pi w^2} \exp\left(\frac{-2(r^2+a^2)}{w^2}\right) \mathcal{I}_0\left(\frac{4ar}{w^2}\right), \qquad (1)$$

where r is the radial distance of the polar coordinate system and $\mathcal{I}_0$ is the zeroth-order modified Bessel function. For ^{87}Rb atoms, the dipole potential for a linearly polarized light with detuning Δ with respect to the D_2 line such that $\Delta'_{\rm FS} \gg |\Delta| \gg \Delta'_{\rm HFS}$, where $\hbar\Delta'_{\rm FS}$ and $\hbar\Delta'_{\rm HFS}$ are respectively the energy splitting of the fine and hyperfine excited states, is given by [16]

$$U(r) = \frac{2}{3}\frac{\hbar\Gamma^2}{8\Delta}\frac{I(r)}{I_{\rm sat}}, \qquad (2)$$

Γ being the linewidth and $I_{\rm sat}$ the saturation intensity of the transition. For large trap size $a/w \gg 1$, i.e., when the radius is large compared to the waist, Eq. (2) simplifies to the intuitive formula

$$U(r) = U_0 \exp\left(-\frac{2(r-a)^2}{w^2}\right), \qquad (3)$$

where the potential height is given by

$$U_0 = \frac{2}{3}\frac{\hbar\Gamma}{8\sqrt{2}\pi^{3/2}}\frac{\Gamma}{\Delta}\frac{P}{I_{\rm sat} a w}. \qquad (4)$$

When the trap is small, i.e., $a/w < 1$, the two walls of the tube start touching each other and the trap can no longer be described as a box with Gaussian walls, but is well approximated by a harmonic potential

$$U(r) = U_1 + \tfrac{1}{2}m\omega^2 r^2, \qquad (5)$$

where $U_1 = (2/3)\frac{\hbar\Gamma}{4\pi}\frac{\Gamma}{\Delta}\frac{P}{I_{\rm sat}w^2}\exp(\frac{-2a^2}{w^2})$ is the "offset" value of the potential at the center of the trap and $\omega = 2\sqrt{\frac{U_1}{m}}\frac{\sqrt{2a^2-w^2}}{w^2}$ is the trap frequency. Figure 2 shows the radial profile of the time-averaged potential for two trap radii as well as its harmonic approximation. The possibility of controlling the trap frequency by tuning its radius can allow for runaway evaporative cooling by compensating the reduction of the trap frequency due to the lowering of the potential barrier (reducing the intensity or increasing the detuning) by a reduction of the size of the trap. The trap frequency is very sensitive to the trap radius. A careful control of the approach to the final trap radius is thus required when reaching the harmonic regime.

B. Laser system

The laser system consists of a distributed-feedback (DFB) laser diode injecting a semiconductor laser amplifier SACHER delivering up to 1 W. After the optical isolator, the beam (power 900 mW) is coupled into a large-core (10 μm), monomode, polarization-maintaining photonic crystal fiber (NKT Photonics LMA-PM-10). The coupling efficiency into the fiber is 60%, limited by the quality of the laser mode of the semiconductor amplifier.

At the output of the fiber, 550 mW of collimated linearly polarized light injects the crossed AOMs, yielding 250 mW in the (+1, +1) diffraction order for creating the light tube. The power of the beam can be controlled by adjusting the rf power driving the AOMs. The light frequency ν can be tuned over 120 GHz without mode jump by adjusting the current I of the

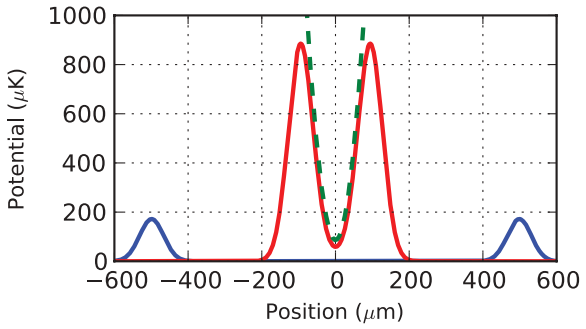

FIG. 2. (Color online) Radial profiles of the time-averaged potential for two trap radii. The solid curves correspond to Eqs. (1) and (2) for trap radii $a = 500\,\mu$m (blue, outer peaks) and $a = 100\,\mu$m (red, inner peaks). The green dashed line represents the harmonic approximation of the potential [see Eq. (5)] for $a = 100\,\mu$m. It gives $U_1 = 85\,\mu$K and $\omega/(2\pi) = 860$ Hz. The parameters are $P = 200$ mW, $\Delta = 40$ GHz, and $w = 65\,\mu$m.

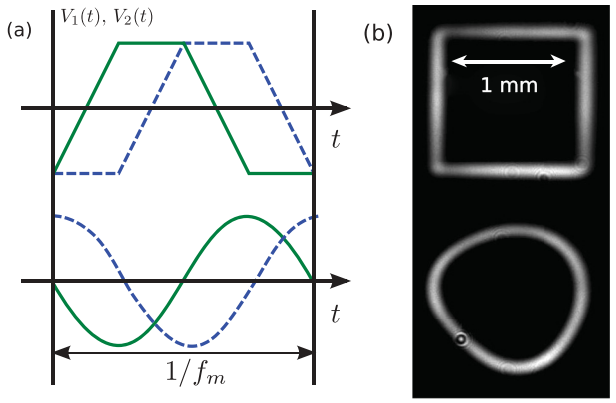

FIG. 3. (Color online) Measured cross sections of the blue-detuned tubes for two different VCO modulations. As an example, we show two useful configurations: the square and the circle. (a) Signals $(V_1(t), V_2(t))$ that are sent to the VCOs. (b) Pictures of the resulting cross sections taken at the position where the atoms are trapped. The size of the trap is $L \simeq 1$ mm and the waist $w = 65$ μm.

DFB diode ($dv/dI = 2$ GHz mA^{-1}). Typical detunings used with this setup range between 5 and 80 GHz.

Such semiconductor laser systems have the advantage of moderate costs and simplicity of implementation. However, they often have a modest mode quality and more importantly they possess an amplified spontaneous emission background which spreads over 40 nm, containing photons at resonance with the atomic line. For experiments where this background spectrum is a limitation, a titanium-sapphire laser or a frequency-doubled laser might be a more convenient choice.

C. Electronic control of rf signals

In order to create the tubes of light, a precise control of the rf signals feeding the AOMs is necessary. For this, we use voltage-control oscillators (VCOs) delivering rf signals whose instant frequencies $f_i(t)$ linearly depend on the input voltages $V_i(t)$. Thus, the two input voltages $(V_1(t), V_2(t))$ are associated with a position $(x(t), y(t))$ in the $(+1, +1)$ diffraction order of the AOMs, such that it is possible to create tubes of light with arbitrary cross sections. Figure 3 shows the signals $V_i(t)$ which produce circular and square tubes as well as the subsequent experimental pictures of these cross sections. We use homemade VCOs, based on the Mini-Circuit POS-150+ chip with output frequency between 50 and 150 MHz and a 3 dB input modulation bandwidth of 100 kHz. Two phase-locked Agilent 33220A function generators are used to drive the VCOs. The VCOs are feeding two Mini-Circuit ZHL-1A rf amplifiers.

In Fig. 3(b), we notice that the ring-shaped potential is slightly asymmetric. We attribute this to nonlinearities in the overall system response $(x(V_1(t)), y(V_2(t)))$ which is supported by the fact that this asymmetry is reduced for smaller traps since they require lower modulation amplitudes. The square-shaped trap is not affected because its parametric equations do not lead to a combined motion in the x and y directions (the nonlinearities imply only that the straight lines are not drawn at constant speed). By designing and engineering the synthesizer signals driving the VCOs, it would be possible to compensate for the trap asymmetry. However, all the measurements performed in this paper use the ring-shaped potential without compensating for the asymmetry, to keep the system complexity to a minimum.

D. Parameters and experimental sequence

Unless otherwise stated, the parameters of the trap are as follows: size $L = 1$ mm (radius $a = 500$ μm), waist $w = 65$ μm, detuning $\Delta = 40$ GHz, rotation frequency $f_m = 90$ kHz, laser power for a single tube $P = 200$ mW, linear polarization. For these parameters, the potential height for ^{87}Rb atoms is 190 μK [see Eq. (4)].

We first load a MOT of ^{87}Rb atoms from a vapor cell with a background gas pressure of $\sim 10^{-9}$ mbar. All lasers are tuned close to the D_2 line of ^{87}Rb and are derived from DFB diodes, conveniently amplified with a tapered amplifier and controlled via AOMs. In this series of experiments, we deliberately choose to work with a moderate number of atoms to investigate the performances of our trapping scheme. We trap $\sim 5 \times 10^7$ atoms in 2.5 s. The loading time can be reduced by increasing the rubidium background pressure when a larger atom number needs to be trapped using, e.g., ultraviolet light-emitting diodes to temporarily increase the hot gas pressure during the MOT loading—so-called light-induced atomic desorption (LIAD) [24,25]. The cooling laser detuning is -3Γ and the temperature of the cloud is ~ 55 μK. We then apply a 50 ms temporal dark MOT period where the intensity of the repumping laser is reduced by a factor of 10 and the detuning of the cooling beam is increased from -3Γ to -6Γ. This allows us to compress and produce a homogeneous distribution of atoms, mainly in the $F = 1$ hyperfine ground state, with a density $\sim 10^{11}$ cm^{-3} and a temperature ~ 20 μK. During the temporal dark MOT period, the intensity of the dipole trap is progressively ramped up in order to maximize the "mode matching" between the dark MOT and the dipole trap. After this, the magnetic field and the laser cooling beams are turned off. In order to keep the atoms in a single hyperfine level, we choose to keep the repumping laser on at all times after loading, thus forcing the atoms into the $F = 2$ hyperfine level.[1] Then the atoms evolve freely in the dipole potential and the trapping time varies between 5 ms and 1.2 s. Using absorption or fluorescence imaging techniques, the properties of the cloud, e.g., the number of atoms, temperature, and density, are measured. In the following, unless otherwise stated, absorption imaging from the side of the cell is used to perform quantitative measurements. Figure 4 shows *in situ* fluorescence images of the cloud taken from the top of the cell for a single tube and for the crossed dipole trap.

III. LOADING

The loading period corresponds to the transfer of the atoms from the dark MOT to the dipole trap. During the first

[1]Pumping the atoms into the $F = 1$ hyperfine level would instead require the development of a specific depumping laser. Indeed, keeping the MOT cooling beams on to pump the atoms in the $F = 1$ hyperfine level would not be efficient and would lead to several scattered photons, thus preventing us from attaining our goal of reaching high densities.

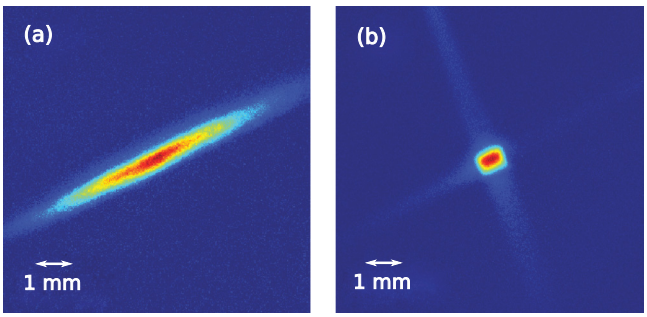

FIG. 4. (Color online) *In situ* fluorescence images of the atoms in the dipole trap taken from the top of the cell after 100 ms of holding time. (a) Single-tube trap. (b) Crossed trap. Parameters: $P = 200$ mW, $\Delta = 40$ GHz, $L = 1$ mm, $w = 65$ μm, and $f_m = 90$ kHz.

∼60 ms, the atoms are in a transient regime before reaching a quasisteady regime. In order to optimize the transfer efficiency from the dark MOT to the dipole trap, it is important to understand the mechanisms occurring during this stage.

A. Transient regime

During the transfer of the atoms from the dark MOT to the dipole trap, the mode matching is not perfect, exciting breathing modes and oscillations of the center of mass of the cloud. Figure 5 shows the center-of-mass position and the root-mean-square (rms) size of the cloud after a 5 ms time of flight as a function of the holding time in the dipole trap. We notice that the cloud is squeezed along the direction of gravity [smaller rms size in Fig. 5(b)] as can also be seen on the *in situ* images (see Fig. 7). We observe oscillations of the cloud size that we identify as *breathing modes*. Their period is similar to that observed on the center-of-mass position. The oscillation period is ∼25 ms, which is compatible with atoms falling from a height $h = 500$ μm and bouncing on the bottom of the trap with a period $2\sqrt{2h/g} \sim 20$ ms. The damping of the oscillations is important because of the strong trap anharmonicity. After ∼60 ms, the oscillations are almost completely damped and the trap enters the so-called *quasisteady regime*.

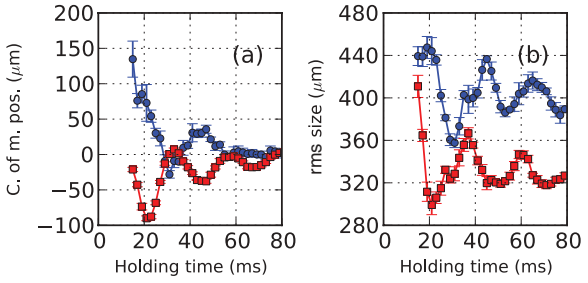

FIG. 5. (Color online) Center-of-mass position (a) and rms size (b) of the cloud after a 5 ms time of flight as a function of the holding time in the dipole trap. The blue points correspond to measurements along the x axis, which is orthogonal to the direction of gravity. The red squares represent measurements along the z axis, which is defined as pointing opposite to gravity. This figure shows center-of-mass oscillations and breathing modes during the transient regime. Parameters: $P = 200$ mW, $\Delta = 40$ GHz, $L = 1$ mm, $w = 65$ μm, and $f_m = 90$ kHz.

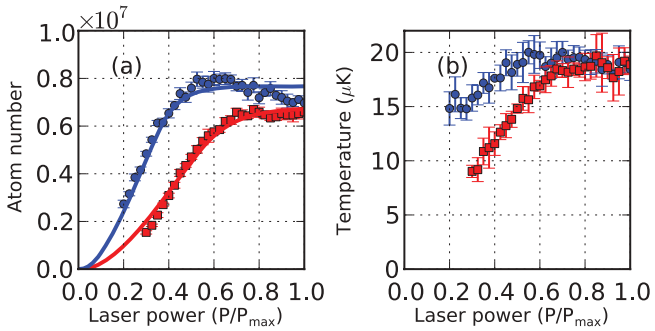

FIG. 6. (Color online) Number of atoms (a) and cloud temperature (b) measured 60 ms after loading as a function of the laser power ($P_{\max} = 200$ mW). The blue points correspond to a detuning of 20 GHz and the red squares to $\Delta = 40$ GHz. The solid lines in (a) are fits of the data according to Eq. (7) using the potential barrier height U as the only free fitting parameter. We obtain $U = 320$ μK for $\Delta = 20$ GHz and $U = 190$ μK for $\Delta = 40$ GHz. Parameters: $L = 1$ mm, $w = 65$ μm, and $f_m = 90$ kHz.

B. Trapped atom number

At the end of the transient regime, ∼60 ms after the atom transfer from the dark MOT, we study the number of trapped atoms and the temperature of the cloud as a function of the laser power, which can be adjusted between 0 and 200 mW. Figure 6 shows the data for two different laser detunings $\Delta = 20$ GHz (blue points) and $\Delta = 40$ GHz (red squares). The trap is loaded from a dark MOT with $\simeq 1.3 \times 10^7$ atoms and a temperature of $\simeq 22$ μK. The size of the trap is $L \simeq 1$ mm.

Both the number of atoms and the temperature reach a plateau after $P = 0.5 P_{\max}$ for $\Delta = 20$ GHz and $P = 0.7 P_{\max}$ for $\Delta = 40$ GHz. The temperature plateau corresponds to the temperature of the dark MOT. This can be understood by noticing that when the barrier height is sufficiently high, all the atoms (initially in the trapping region) are trapped and their temperature is that of the dark MOT. Before the plateau, the temperature increases linearly with laser power, which can be understood as a consequence of the linear increase of the potential barrier with laser power. The red squares in Fig. 6(b) clearly point at the origin when $P \to 0$, which is consistent with the fact that only atoms with an energy (kinetic plus potential) smaller than the barrier height are trapped during loading. However, the blue points do not extend to the origin when $P \to 0$, which might be due to spontaneous-emission heating, which is more important for a detuning of 20 GHz than for 40 GHz.

We define the loading efficiency as the number of atoms in the trap after 60 ms of holding time (i.e., at the end of the transient regime) divided by the number of atoms in the dark MOT measured before loading. For the data presented on Fig. 6, the loading efficiency is 60%, which corresponds to an excellent value compared to what is usually observed in red-detuned dipole traps. When the size of the dark MOT is smaller than the trap volume, the nontrapped atoms correspond to those having a too large energy (kinetic plus potential): they "jump" over the potential barrier. If gravity were compensated (by, e.g., optical pumping of the atoms in a particular Zeeman sublevel and applying a vertical magnetic field gradient), the atoms would possess only kinetic energy, which should

significantly improve the loading efficiency. The maximum estimated number of atoms that can be trapped is $\sim 10^8$ (equal to the density of the dark MOT, $\sim 10^{11}$ cm^{-3}, times the trapping volume, ~ 1 mm^3).

1. *Model for trap loading*

We consider the case of a box-shaped trap and suppose that in the dark MOT, the atoms are uniformly distributed in space, with a momentum probability distribution given by the Boltzmann distribution

$$p(\mathbf{p},\mathbf{r}) = \frac{\Lambda_T^3}{L^3} \exp\left[-\frac{\mathbf{p}^2}{2mk_BT}\right],$$

where $\Lambda_T = h/\sqrt{2\pi m k_B T}$ is the thermal wavelength. The probability density for an atom to have an energy E is $p(E) = \int \frac{d^3\mathbf{p}\,d^3\mathbf{r}}{h^3}\delta(E(\mathbf{p},\mathbf{r}) - E)p(\mathbf{p},\mathbf{r})$, where the energy of the atom takes the form $E(\mathbf{p},\mathbf{r}) = \mathbf{p}^2/(2m) + mgz$, with the z axis defined along the direction opposite to gravity. After some calculations, we find

$$p(E) = \frac{2}{\sqrt{\pi}k_BT}\sqrt{\frac{E}{k_BT}} \exp\left[-\frac{E}{k_BT}\right] \mathcal{F}\left(\frac{E}{mgL}, \frac{mgL}{k_BT}\right), \quad (6)$$

where the function $\mathcal{F}$ is defined as $\mathcal{F}(\alpha,\beta) = \int_0^{\min(\alpha,1)} du\sqrt{1-u/\alpha}\,\exp(\beta u)$. In the $g \to 0$ case, i.e., without gravity, Eq. (6) simplifies to the well-known free-space density probability $p(E) = 2/(\sqrt{\pi}k_BT)\sqrt{E/(k_BT)}\exp[-E/(k_BT)]$, where in front of the Boltzmann factor $\exp[-E/(k_BT)]$ one recognizes the three-dimensional free-space density of states. If the height of the potential barrier is U, then the fraction of atoms N/N_0 that are trapped during loading is given by

$$\frac{N}{N_0} = \int_0^U dE\, p(E). \quad (7)$$

The solid lines in Fig. 6 correspond to fits according to Eq. (7) which allows us to determine, using a single free fitting parameter, the potential height U corresponding to $P_{\max} = 200$ mW. We obtain $U = 320$ μK for $\Delta = 20$ GHz and $U = 190$ μK for $\Delta = 40$ GHz. We can compare these values to theoretical estimations by substituting the experimental parameters into Eq. (4), leading respectively to $U = 380$ and 190 μK, in good agreement with the values extracted from the fit.

IV. QUASISTEADY REGIME

After the transient regime leading to the loading of the trap, the evolution of the cloud properties occurs on a longer time scale: the quasisteady regime. In this section, we study the evolution of the cloud in this quasisteady regime in order to characterize the trap and to understand the mechanisms limiting its performance. To this end, two quantities are of particular interest: the trap lifetime and the temperature of the cloud. The lifetime τ is determined from an exponential fit $N_0\exp(-t/\tau)$ to the decay curve of the number of atoms in the trap as a function of the holding time, while the temperature is inferred from the rms size of the cloud measured in time of flight.

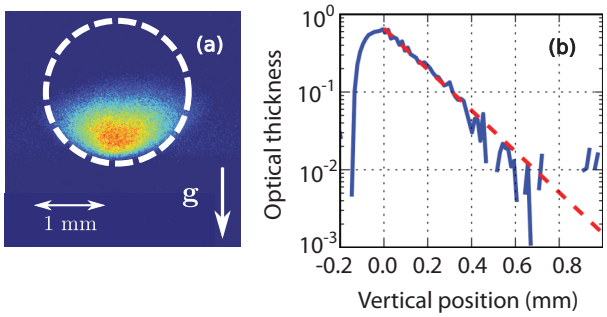

FIG. 7. (Color online) (a) *In situ* absorption image of the cloud inside the dipole trap 450 ms after loading (sideview). The white dashed line represents the limits of the trap. The atoms lie down on the bottom of the trap due to gravity. (b) Vertical optical thickness profile (blue solid curve). The origin is chosen at the position of the maximum optical thickness. The fit $b(z) = b(0)\exp[-mgz/(k_BT)]$ (red dashed line) leads to a temperature of 18 μK. The temperature estimated using the standard time of flight measurement gives 21 μK. Parameters: $P = 200$ mW, $\Delta = 40$ GHz, $L = 1$ mm, $w = 65$ μm, $f_m = 90$ kHz.

A. *In situ* density profile

For a trap of size L, gravity effects can be neglected when $mgL \ll k_BT$. For a cloud temperature of 40 μK, this condition gives $L \ll 400$ μm, showing that gravity is an important parameter for large traps. The influence of gravity can be observed in the absorption imaging from the side of the chamber as shown in Fig. 7 where atoms lie down on the bottom of the trap. This situation is similar to that observed with strontium MOTs on the intercombination line at 689 nm [26].

For atoms at thermal equilibrium in the dipole trap, one expects the optical thickness profile along the vertical direction to be given by the Boltzmann factor

$$b(z) = b(0)\exp\left[-\frac{mgz}{k_BT}\right]. \quad (8)$$

Figure 7 shows the *in situ* density profile of the cloud obtained by absorption imaging. A fit from Eq. (8) leads to a temperature of 18 μK. The temperature of the cloud given by a time-of-flight measurement is 21 μK, in good agreement with the *in situ* measurement. As one does not expect a thermodynamic equilibrium to be reached when considering the conservative dynamics of independent particles in a trap, the good agreement between these two methods of estimating the temperature of the atomic cloud suggests that relaxation due to residual light scattering combined with a limited trap height or "s-wave" collisions (the elastic s-wave collision rate after loading is $\Gamma_{\rm el} \lesssim 10$ s^{-1}) might be present in our system.

B. Losses due to "hot" collisions

The MOT loading time of ~ 20 s allows us to infer a background gas pressure of $P \sim 10^{-9}$ mbar [27]. The trap loss rates due to the background species i can be estimated

TABLE I. Coefficients C_i of the van der Waals potential between rubidium and background species i in Hartree atomic units (a.u.) = $e^2a_0^5/(4\pi\epsilon_0)$, where e is the electron charge, a_0 is the Bohr radius, and ϵ_0 is the vacuum permittivity (data taken from Ref. [29]). Trap loss rate γ_i computed from Eq. (9) with $P_i \simeq 10^{-9}$ mbar, $U = 190\ \mu$K, and $T = 300$ K.

Species i	C_i (a.u.)	γ_i (s^{-1})
Rb-Rb	4430	0.14
Rb-He	36.2	0.08
Rb-H_2	140	0.16

by [27–29]

$$\gamma_i \simeq 6.8\frac{P_i}{(k_BT)^{2/3}}\left(\frac{C_i}{m_i}\right)^{1/3}(Um_{\mathrm{Rb}})^{-1/6}, \qquad (9)$$

where $T \simeq 300$ K is the background gas temperature, P_i the partial pressure of the background species i, and $U \simeq 190\ \mu$K the potential height of the dipole trap. With m_{Rb} and m_i we indicate the masses of rubidium and of the background species, i and C_i are the coefficients of the van der Waals interaction potential $-C_i/r^6$ between the ground-state trapped Rb atoms and i. Table I gives the value of the C_i coefficients for Rb-Rb, Rb-He, and Rb-H_2 collisions and the corresponding trap loss rates γ_i for the parameters of the experiment. The estimated trap lifetimes $1/\gamma_i$ resulting from the background collisions are significantly longer than the measured one, allowing us to conclude that the dominant loss mechanism is not due to collisions with the background gas.

A further confirmation of the marginality of hot collisions is obtained by performing a lifetime measurement by turning on LIAD just after loading the trap. Even though this increases the residual gas pressure of the cell by one order of magnitude to $P \sim 10^{-8}$ mbar, we notice no difference on the measured lifetime.

C. Influence of the trap size

The influence of the size of the trap on its lifetime is an important issue to study before starting the compression of the cloud. After loading, the atoms are kept in the trap for 20 ms, before linearly reducing the trap size for an additional 20 ms. The end of this stage is used as the initial condition to measure the lifetime of the cloud. We choose this experimental procedure since it allows an efficient trap loading and prevents nontrapped atoms (because of the too small trap volume compared to the dark MOT volume) from being present in the imaging region when the trapped atom number is measured during the first 40 ms. The initial conditions are chosen such that the initial atomic density is low enough to prevent density effects in the measurement (small s-wave collision rate). Note that this experimental procedure does not maintain the potential height constant, as $U \propto 1/L$ [see Eq. (4)].

Figure 8 shows that the lifetime of the cloud rapidly decreases when the size of the trap is reduced. This is consistent with atom losses occurring when the atoms interact with the potential barrier. The smaller is the trap, the more frequent are interactions with the barrier, leading to stronger losses and to a subsequent lifetime reduction. The reduction of the lifetime

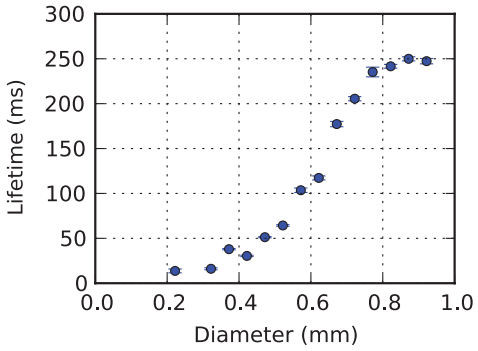

FIG. 8. (Color online) Lifetime of the cloud as a function of the dipole trap diameter. Parameters: $P = 200$ mW, $\Delta = 40$ GHz, $w = 65\ \mu$m, and $f_m = 90$ kHz.

with the trap size is an important factor to take into account for the cloud compression.

D. Influence of the rotation frequency

A first limiting effect gives a lower bound for low rotation frequencies: if during one period $1/f_m$, the atoms with velocity on the order of $\sim\sqrt{k_BT/m}$ move by more than the waist of the laser w, the atom can escape the trap between successive arrivals of the laser beam. This condition is written

$$f_m \gg \frac{1}{w}\sqrt{\frac{k_BT}{m}} \simeq 1\ \mathrm{kHz}, \qquad (10)$$

for $w = 65\ \mu$m and $T = 40\ \mu$K.

In order to study the influence of the rotation frequency above this limit, we vary the rotation frequency and keep all other parameters constant. Figure 9(a) shows that the lifetime increases with increasing rotation frequency without reaching saturation in the explored frequency range (contrary to what is observed in Ref. [17]). This can be understood by noticing that the faster the beam rotates, the better is the time-averaged-potential approximation. The upper bound for the rotation frequency is set by the input modulation bandwidth of the VCOs.

Figure 9(b) shows the cloud temperature after 150 ms of holding time as a function of the rotation frequency. Below 30 kHz, we observe significant heating which decreases with increasing rotation frequency. Above 30 kHz, the temperature

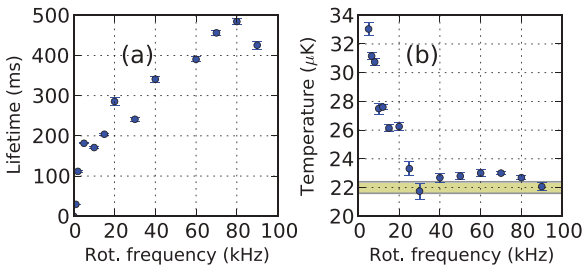

FIG. 9. (Color online) (a) Lifetime of the dipole trap as a function of the rotation frequency. (b) Temperature of the cloud measured after 150 ms of holding time as a function of the rotation frequency. The shaded area represents the initial dark MOT temperature before loading the dipole trap. Parameters: $P = 200$ mW, $\Delta = 40$ GHz, $L = 1$ mm, and $w = 65\ \mu$m.

reaches a plateau which is close to the initial dark MOT temperature [shaded area in Fig. 9(b)]. We identify this phenomenon as being due to dipolar heating, i.e., heating due to the dipole potential fluctuations that atoms experience when they bounce on the potential barrier because of the rotating laser. From this measurement, we can get an estimate of the dipole-induced heating rate, expected to scale as $1/(Lf_m)$, which can be used for optimizing compression schemes.

After compression, for small trap size in the harmonic regime, we also require the rotation frequency to be large compared to the trap frequency $\omega/(2\pi)$ for the time-averaged approximation to be valid. The maximum trap frequencies that can be reached are a few kilohertz. By using a rotation frequency close to 100 kHz the two previous conditions are easily satisfied.

It is clear that the trap has better performance when the rotation frequency is increased. However, there is an intrinsic limitation that restrains this argument. Indeed, modulatation of a signal at a frequency f_m creates sidebands separated by f_m. These sidebands affect the dipole potential. The limit for having a nice "continuous trap shape" is to consider that the distance d between two peaks associated with two sidebands should be smaller than the laser waist $w = 65\ \mu$m. The AOM deflection angle is $\alpha = 9.3 \times 10^{-5}$ rad MHz^{-1}, and after a distance $L = 150$ mm (the lens focal length), the distance between two points is $d = \alpha f_m L$. The condition is then written

$$f_m \ll \frac{w}{\alpha L} \simeq 5\ \text{MHz}. \tag{11}$$

This argument shows that there is an intrinsic limit for the maximum frequency one can use. However, we are limited to $f_m < 100$ kHz by the VCOs, so there is still room for improvement.

In summary, below a modulation frequency of ~1 kHz, the atoms are no longer trapped. This regime can be observed in the two first points of Fig. 9(b). In the intermediate regime $3 < f_m < 30$ kHz, we observe a reduction of the heating. This regime is associated with dipolar heating losses due to the rotating laser. For $f_m > 30$ kHz we observe an increase of the lifetime and a stabilization of the temperature. These results justify the choice of a rotation frequency of 90 kHz, which corresponds to the maximum frequency we can use, taking into account the 100 kHz input modulation bandwidth of the VCOs. The performance of the trap might probably be improved using VCOs with a higher input modulation bandwidth and a better frequency stability.

E. Influence of the detuning

We study the influence of the detuning on the lifetime and temperature by changing Δ and P while maintaining $U \propto P/\Delta$ constant. The first point on the right side of Fig. 10 is measured for $P = 200$ mW and $\Delta = 60$ GHz, corresponding to a potential height $U = 126\ \mu$K.

Figure 10(a) shows that for $\Delta < 20$ GHz the lifetime strongly depends on the detuning, and that for $\Delta > 20$ GHz, the lifetime becomes constant at ~280 ms. It is important to note that the semiconductor laser diodes used in these experiments present, in addition to their main laser mode, a pedestal which spreads over 40 nm. From the data of Fig. 10(a), we

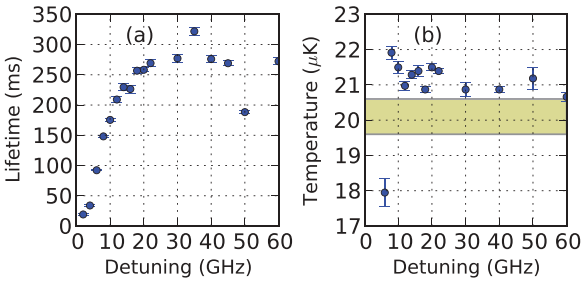

FIG. 10. (Color online) (a) Lifetime of the dipole trap as a function of the laser detuning at constant potential height. For this measurement we adjust the laser power to maintain a constant potential barrier $U \propto P/\Delta$ while the detuning is varied. (b) Temperature of the cloud measured after 150 ms of holding time as a function of the laser detuning. The shaded area represents the initial dark MOT temperature before loading the dipole trap. Parameters: $L = 1$ mm, $w = 65\ \mu$m, and $f_m = 90$ kHz.

conclude that above 20 GHz spontaneous emission due to the main laser mode is not the limiting phenomenon leading to atom losses. We attribute the limited lifetime above 20 GHz to heating induced by the amplified spontaneous-emission pedestal and dipolar heating as discussed in Sec. IV D.

In Fig. 10(b), we notice that the cloud temperature does not depend on the laser detuning. The temperature is constant, slightly higher than the dark MOT temperature. After loading the cloud at the dark MOT temperature spontaneous emission leads to atom losses without temperature increase (the potential height is $126\ \mu$K). We conclude that the extra heating due to spontaneous emission is immediately suppressed by evaporation: the atoms escape from the trap when their total energy becomes higher than the potential barrier height.

We notice in Fig. 10(a) particularly short trap lifetimes around $\Delta = 50$ GHz. In order to study this more quantitatively, we measure the number of atoms in the dipole trap after 150 ms of holding time using the same experimental parameters as in Fig. 10. These data points are shown in Fig. 11 where we observe a 10 GHz broad resonance centered around 50 GHz which manifests itself as atom losses. No resonance is seen

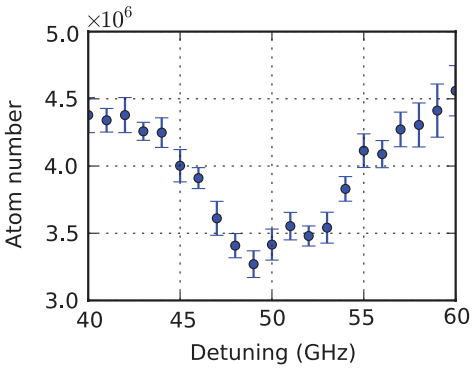

FIG. 11. (Color online) Number of atoms in the dipole trap after 150 ms of holding time as a function of the laser detuning at constant potential height. This curve shows a region where we measure abnormally low lifetimes, which indicates a resonance whose origin is unknown. The resonance is centered around 50 GHz and is 10 GHz broad. Parameters: $L = 1$ mm, $w = 65\ \mu$m, and $f_m = 90$ kHz (the same as those of Fig. 10).

in the incident laser spectrum and its origin remains elusive. Possible explanations might involve acoustic modes in the optical fiber or, more interestingly, molecular resonances.

F. Influence of the laser system spectrum

Assuming thermal equilibrium, the mean photon scattering rate Γ_{sc} can be estimated from the temperature by computing the average potential

$$\langle U\rangle = \frac{\int d\mathbf{r}\, U(\mathbf{r}) \exp\left[-\frac{U(\mathbf{r})+mgz}{k_B T}\right]}{\int d\mathbf{r}\, \exp\left[-\frac{U(\mathbf{r})+mgz}{k_B T}\right]}, \tag{12}$$

and using the relation $\hbar\Gamma_{sc} = U\,\Gamma/\Delta$. For a blue dipole trap $\langle U\rangle$ and $\langle\Gamma_{sc}\rangle$ are both increasing functions of the temperature. For the typical parameters of the experiment, $P = 200$ mW, $\Delta = 40$ GHz, $L = 1$ mm, $w = 65\ \mu$m, and $T = 20\ \mu$K, evaluation of Eq. (12) gives $\langle U\rangle = 2.11\ \mu$K and $\langle\Gamma_{sc}\rangle = 41\ \mathrm{s}^{-1}$. This underestimates the photon scattering rate by not accounting for imperfections of the potential. More importantly, a major drawback of semiconductor laser systems is their amplified spontaneous-emission background which spreads over 40 nm and contains photons resonant with the atomic lines. These photons contribute to heating, leading to a potential reduction of the trap lifetime. The spontaneous-emission background is clearly seen when looking at the laser system power spectrum shown in Fig. 12(a). It represents 0.9% of the total laser power. In this section, we investigate two different approaches to filtering resonant photons using an etalon or a rubidium cell.

The first method consists in filtering the spontaneous-emission background using an etalon of finesse $\mathcal{F} = 60$ with free spectral range $\Delta\nu_{FSR} = 210$ GHz. Its transmission exhibits peaks separated by 210 GHz with full with at half maximum $\Delta\nu_{FSR}/\mathcal{F} = 3.5$ GHz. For an optical spectrum analyzer that does not resolve the transmission peaks, the expected reduction of the spontaneous emission background is $10\log_{10}\mathcal{F} = 17$ dB, which shows good agreement with the measurements presented in Fig. 12(a). After filtering, the spontaneous emission background represents only 0.04% of the total laser power. Due to the poor mode quality of the laser system, the coupling efficiency through the etalon is weak, leaving only 70 mW of light available for creating the dipole trap. In order to maintain a decent trap depth, we reduce the laser detuning to 24 GHz. The influence of the filtering on the trap lifetime is shown in Fig. 12(b). The measurement indicates that the spontaneous-emission background is not the dominant effect which limits the trap lifetime below 200 ms.

The second method involves using a 7.5-cm-long rubidium cell to filter photons around the Doppler-broadened lines. Heating the cell from 22 to 120 °C allows the filtering of photons by increase in the rubidium pressure of several orders of magnitude. Using heated cells as narrowband absorption filters to reduce the amplified spontaneous-emission background of diode laser systems has proven to be an efficient technique to minimize resonant photon scattering in dipole traps, hence extending their lifetimes [30–32]. Figure 12(c) illustrates the filtering efficiency by looking at the transmission of a weakly saturating probe through the cell. Figure 12(d) shows the number of atoms in the trap as a function of time with

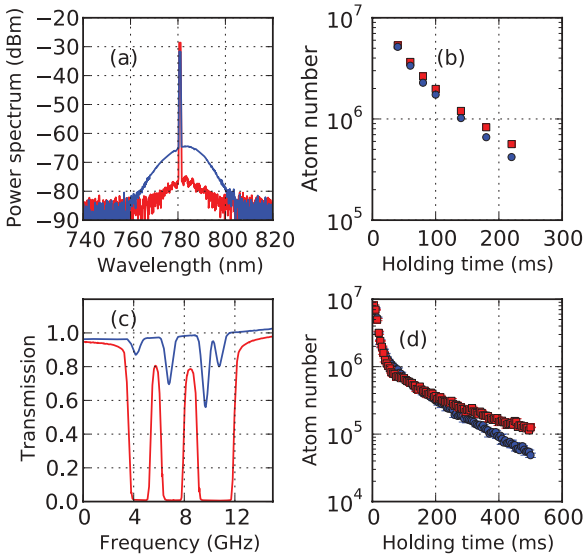

FIG. 12. (Color online) (a) Power spectrum of the laser system (blue, broader, curve) and of the laser system plus etalon (red curve). (b) Number of atoms in the dipole trap as a function of the holding time without (blue points) and with etalon (red squares). The lifetimes are 58 and 66 ms, respectively. The laser power is the same for the two measurements. Parameters: $P = 70$ mW, $\Delta = 24$ GHz, $L = 1$ mm, $w = 65\ \mu$m, and $f_m = 90$ kHz. (c) Transmission of a weakly saturating probe through a 7.5-cm-long rubidium cell at 22 °C (blue, upper, curve) and 120 °C (red curve). (d) Number of atoms in the dipole trap as a function of the holding time using the rubidium cell at 22 °C (blue points) and 120 °C (red squares). Parameters: $P = 200$ mW, $\Delta = 43$ GHz, $L = 1$ mm, $w = 65\ \mu$m, and $f_m = 90$ kHz.

and without filtering. These curves show a double-exponential decay. We relate the first decay to losses occurring during the transient regime and the second one to losses in the quasisteady regime where the lifetime of the trap is evaluated. Again, below 200 ms we are not able to observe any benefit from resonant photon filtering. However, for longer trapping times, we notice lower atom losses, indicating that photon scattering from the spontaneous-emission background becomes important.

In conclusion, below 200 ms, light scattering from the laser pedestal does not limit the experiment. Since we are aiming at fast compression times, we choose not to use any filtering method in the setup. Nevertheless, our data indicate that one should definitely consider implementing these techniques to obtain long trapping times, which might be useful in applications involving quantum-degenerate gases.

G. Conclusion and final performance

The dipole trap presented in this section allows for trapping a large number of atoms with an excellent loading efficiency. Table II summarizes the performance and limitations of the setup. It helps us find the best compromise for our purposes with the following parameters that maximize the loading, the lifetime, and the cloud temperature: $P = 200$ mW, $\Delta = 40$ GHz, $L = 1$ mm, $w = 65\ \mu$m, and $f_m = 90$ kHz. With these parameters, the height of the potential barrier is $\sim$190 μK, the typical lifetime is $\sim$450 ms, and the temperature

TABLE II. Summary of the experiments performed on the static dipole trap in the quasisteady regime. For each measurement, we identify a mechanism leading to losses and/or heating and find the parameters that give the best trap performances.

Experimental parameters	Losses and/or heating mechanisms	Solutions
Size L	Interactions with potential barrier	Largest possible size ∼1 mm for better lifetime and loading
Rotation frequency f_m	Dipolar heating	$f_m > 30$ kHz, the largest possible keeping in mind the sideband limit. Limited by the VCO modulation bandwidth: 90 kHz.
Laser mode detuning Δ	Spontaneous emission	$\Delta > 20$ GHz, ideally the largest possible while keeping a suitable potential height
Laser system pedestal	Spontaneous emission	Beam filtering through etalon or rubidium hot cell

of the cloud is constant at ∼25 μK (about the dark MOT temperature), leading to a factor $\eta = U/(k_B T) \simeq 7.6$.

V. COMPRESSION

In this section, we compress the atomic cloud by dynamically reducing its size L by means of the blue-detuned crossed dipole trap. The goal is to quickly compress the maximum number of atoms N below the strong localization threshold, qualitatively given by the Ioffe-Regel criterion [13]. As discussed in the Introduction, this threshold corresponds to atomic densities of $n = N/L^3 \simeq 10^{13}$–10^{14} cm^{-3} for rubidium atoms.

A. Principles of the compression scheme

The aim of this section is to understand the relevant parameters for compressing the cloud. Simple arguments allow us to qualitatively address important issues, even though they do not aim at describing the experiment in a rigorous way (in particular concerning the role of gravity).

1. Maximum compression speed

We are interested in calculating the maximum speed at which the potential barrier of height U can move before the atoms are no longer able to follow the motion of the barrier and consequently jump over it. Let us consider the most pessimistic case where the potential barrier moves towards the atoms in the laboratory frame at a speed $v_{\rm pot}$ while the atom moves in the opposite direction at a speed $v_{\rm atom}$. In the frame attached to the potential barrier, the atom has a velocity $v = v_{\rm pot} + v_{\rm atom}$ and will not jump over the barrier if its kinetic energy is smaller than the potential height, leading to the criterion $v_{\rm pot} < \sqrt{2U/m} - v_{\rm atom}$. Noting that $\sqrt{2U/m} \gg v_{\rm atom}$, the condition simplifies to

$$v_{\rm pot} < \sqrt{\frac{2U}{m}}. \tag{13}$$

For a 200 μK potential height, we obtain a maximum barrier velocity of 0.2 m s^{-1}. If the barrier moves by 500 μm, the minimal time needed to compress the cloud is 2.5 ms. This will not be a restrictive constraint for the experimental realization of the compression. Moreover, knowing that the potential barrier increases during compression [cf. Eq. (4)], Eq. (13) overestimates the minimum compression time.

2. Heating

For an ideal gas undergoing an adiabatic reversible process the following equation applies: $TV^{\gamma-1} = \text{const}$, where T is the temperature, V the volume, and γ the adiabatic index. For a monatomic gas $\gamma = 5/3$. When the size of the trap is reduced to L_f, a cloud of monatomic atoms (e.g., rubidium atoms) initially at a temperature T_i in a trap of size L_i will reach a temperature T_f given by

$$\frac{T_f}{T_i} = \left(\frac{L_i}{L_f}\right)^2. \tag{14}$$

Any nonadiabatic reversible compression would lead to higher final temperatures than the one predicted by Eq. (14).

3. Phase-space density evolution

When the size of the trap is reduced such that $a \simeq w$, i.e., the radius is about equal to the waist, the geometry of the trap changes from a box with Gaussian walls to a harmonic potential $U = U_1 + (1/2)m\omega^2 r^2$ where the analytical expressions for U_1 and ω are given in Sec. II A. During an adiabatic compression, the entropy of the cloud is conserved, implying phase-space density conservation when the geometry of the trap does not change. However, when the geometry of the trap changes from a box to a harmonic potential, the phase-space density ρ slightly increases. Denoting by $\rho_i \equiv n_i \Lambda_{T_i}^3$ (where n_i is the density and Λ_{T_i} is the initial thermal wavelength) the initial phase-space density for the atoms in a box, and by $\rho_f \equiv n_f \Lambda_{T_f}^3$ the final phase-space density for the atoms at the center of the harmonic trap, one can easily show that the increase in phase-space density for an adiabatic transformation is given by[2]

$$\rho_f = e^{3/2}\rho_i. \tag{15}$$

This phase space density increase comes from the modification of the density of states when the trap geometry is modified [33,34].

4. Potential height evolution

The temperature increase of the cloud resulting from the compression tends to make the atoms escape from the trap by jumping over the potential barrier. However, when the trap size

[2]The following equation is obtain by equating the entropy of an ideal gas in a box $S = Nk_B\{\ln[V/N\Lambda_T^3] + \frac{5}{2}\}$ and its entropy in a harmonic trap $S = Nk_B\{\ln[(1/N)(k_B T/\hbar\omega)^3] + 4\}$.

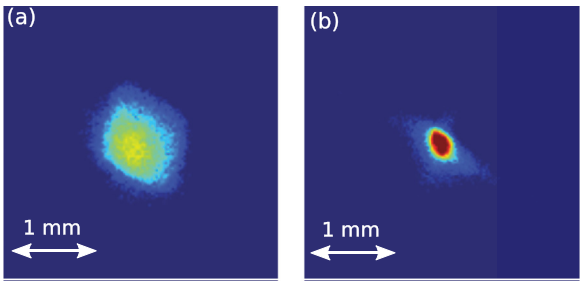

FIG. 13. (Color online) *In situ* fluorescence images of the atoms in the dipole trap taken from the top of the cell. (a) Cloud before compression, trap size $L_i = 1$ mm. (b) Cloud after a 10 ms compression, trap size $L_f = 300$ μm. Parameters: $P = 200$ mW, $\Delta = 40$ GHz, $w = 65$ μm, and $f_m = 90$ kHz.

is reduced, the potential height increases as well. Equation (4) shows that a trap with initial size L_i and potential height U_i, compressed to a final size L_f, has a final potential height $U_f = U_i L_i / L_f$. The temperature of the atoms thus increases faster than the height of the potential. Using Eq. (14), and neglecting collisions (evaporation), atoms stay in the trap while $k_B T_f = U_f$, which allows us to estimate the size of the trap before the atoms escape:

$$\frac{L_f}{L_i} = \frac{k_B T_i}{U_i}. \tag{16}$$

In the experiment $k_B T_i / U_i \sim 1/8$ so that, starting from a trap size of 1 mm, we can compress the cloud down to $\sim$125 μm before atoms jump over the potential barrier.

5. *Lifetime constraint*

In addition to the constraints on the minimum compression time discussed in Sec. V A1, there are also restrictions on the maximum compression time. We have shown in Sec. IV C that the trap lifetime strongly depends on its size. This implies important limitations on the maximum compression time that should be used. For example, using the data from Fig. 8, compressing the cloud to a final size of 400 μm should be done in less than 30 ms (which is the lifetime of the trap for this diameter) in order not to lose too many atoms during compression.

B. Experimental realization

After loading the dipole trap (initial size $L_i = 1$ mm) using the protocol described in Sec. II D, the size of the trap is kept constant during 20 ms in order for the nontrapped atoms to escape from the imaging field of view. The size of the trap is then linearly reduced and the compression time can be varied. The data presented below are taken for different final trap sizes L_f, while the compression time is fixed. Figure 13 shows fluorescence images of the cloud viewed from the top of the cell, before and after compression. Absorption imaging from the side of the trap is used to perform quantitative measurements.

Figure 14 shows the density (a) and the temperature (b) of the cloud as functions of the trap size after compression L_f for two different compression times: 5 ms (blue points) and 10 ms (red squares). The blue points correspond to 2×10^7 initially loaded atoms and the red squares to 10^7 atoms. We manage to increase the density by more than one order of magnitude to reach 5×10^{12} cm^{-3}, reducing the trap size by a factor of 5. Figure 14(b) shows strong heating during compression. The faster the compression, the higher the heating, as expected from the discussion on adiabatic heating in Sec. V A. In the future, if the high final temperature is a problem, one can think of adding an evaporative cooling stage after compression, which would make the cloud colder and denser. We notice that for small compression ($L_f > 0.6$ mm), the density and the temperature are almost unaffected. This can be understood by looking at absorption images of the cloud (see Fig. 7) where the atoms do not occupy the full trap volume because of gravity. The change of slope that we observe for $L_f < 0.6$ mm corresponds to the situation where the cloud starts occupying all the trap volume. For small trap size we observe a saturation of the cloud density when the trap reaches the harmonic regime. This might be due to the the increased sensitivity to instabilities for small traps. Indeed, in the harmonic regime, the trap frequency is very sensitive to the trap size. Inelastic (s-wave or/and light-assisted) collisions can also play a role at high densities and contribute to the observed fluctuations.

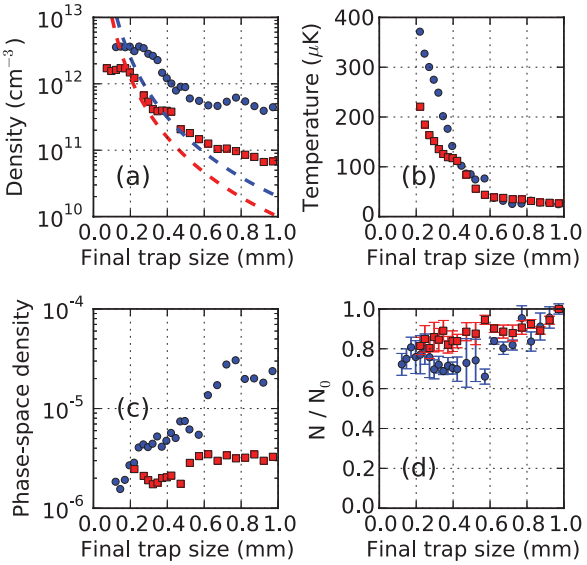

FIG. 14. (Color online) (a) Density, (b) temperature, and (c) phase-space density of the cloud as a function of the trap size after compression L_f. (d) Fraction of the remaining atoms after compression. The initial trap size is $L_i = 1$ mm. The blue points correspond to a 5 ms compression and the red squares to a 10 ms compression. The initial conditions are $N = 2 \times 10^7$ initially loaded atoms for the blue points and $N = 10^7$ atoms for the red squares. The dashed curves in (a) correspond to the densities one would obtain if the trap were uniformly loaded $n = N/L^3$. Parameters: $P = 200$ mW, $\Delta = 40$ GHz, $w = 65$ μm, and $f_m = 90$ kHz.

Figure 14(c) shows the phase-space density $n\Lambda_T^3$ as a function of the final trap size. As previously discussed, the phase-space density is conserved for an adiabatic compression if the trap geometry does not change (the density of states is conserved). We observe that for a 10 ms compression time, the phase-space density is conserved but this is no longer the case when the compression time is 5 ms.

Figure 14 (d) shows the fraction of remaining atoms after compression. We manage to keep more than 80% of the atoms, which is very promising. To do so, we need to compress faster than any loss mechanism; in particular, faster than the trap lifetime for the final trap size we are aiming at (see Fig. 8).

1. Maximum density

The experiments performed above are designed to understand how compression works. They are carried out using a 2.5 s MOT loading time from a low-pressure background gas, resulting in a modest number of atoms loaded into the trap, $\sim 10^7$. Techniques to increase the number of trapped atoms include making the loading time longer, increasing the background gas pressure using LIAD, or enlarging the initial trap volume. The latter is something difficult to achieve with our current setup. Therefore, a cloud with more atoms but a larger initial size would not increase significantly the number of trapped atoms. Improving the dark MOT density (by further detuned trapping lasers) will be important to increase the number of trapped atoms well beyond 10^8.

To test the performance of the trap we simply increase the MOT loading time to 20 s. We also use a detuning of 20 GHz (compared to 40 GHz usually) to increase the potential height. In these conditions, 5×10^7 atoms are loaded into the trap. After compressing the cloud to a final size of 200 μm in 5 ms, we measure a density of 10^{13} cm^{-3}, which corresponds to

$$kl \simeq 2.8, \tag{17}$$

compatible with the Ioffe-Regel criterion. This setup thus proves to be an effective tool to rapidly compress a large atomic cloud down to the strong-localization threshold, paving the way for efficient exploration of light-matter interaction in the dense regime. In the future, the trap performances can be further improved by having a more precise control of the trap-size evolution when the trap enters the harmonic regime, since in this regime the parameters of the trap (e.g., the trap frequency) vary very quickly with its radius.

C. Collisions and thermalization

When the cloud is compressed, the spatial density and the temperature rise, which makes the cloud enter into a regime where collisions are no longer negligible on the time scale of the experiments [35]. The elastic collision rate is given by

$$\Gamma_{\rm el} = n\sigma\bar{v}_{\rm rel}, \tag{18}$$

where n is the cloud density, $\bar{v}_{\rm rel} = 4\sqrt{k_B T/(\pi m)}$ is the mean relative atom velocity, and σ is the total elastic cross section. If we consider pure s-wave collisions, which in our case is a strong approximation given the temperature of the gas (where higher-order collisions, e.g., p-wave collisions, can occur), the total cross section is given by $\sigma = 8\pi a^2$ for identical bosons ($\sigma = 4\pi a^2$ for nonidentical particles), where a is the scattering length. Elastic s-wave collision rates computed for the data of the experiments presented in Sec. V B are shown in Fig. 15(a). During compression, the collision rate increases by almost two orders of magnitude (from 10 to 10^3 s^{-1}). In our compressed trap, s-wave collisions are thus expected to become relevant, with subsequent thermalization and evaporation.

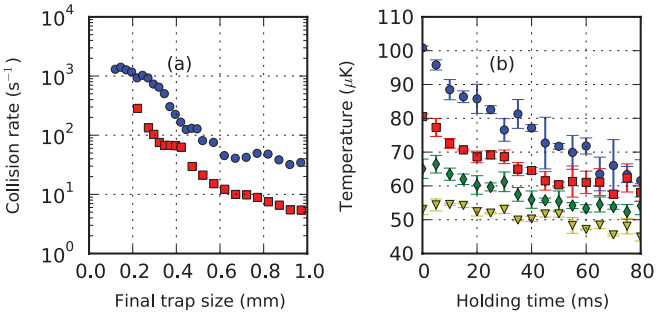

FIG. 15. (Color online) (a) Elastic s-wave collision rate as a function of the trap size after compression. The blue points correspond to a 5 ms compression and 2×10^7 atoms initially loaded. The red squares correspond to a 10 ms compression and 10^7 atoms initially loaded. (b) Temperature as a function of the holding time for different initial conditions of the atoms in the dipole trap. The different initial conditions are prepared by compressing the cloud during 40 ms from an initial size $L_i = 1$ mm to different final trap sizes after compression, $L_f = 0.42$ mm (blue points), 0.47 mm (red squares), 0.52 mm (green diamonds), and 0.57 mm (yellow triangles). After compression the diameter is kept constant. The state of the system after compression is used as the initial condition for this measurement. The smaller is the trap size after compression, the hotter and denser are the cloud initial conditions. The initial densities and temperatures are $1.7 \times 10^{11}, 1.6 \times 10^{11}, 1.4 \times 10^{11}, 1.2 \times 10^{11}$ cm^{-3} and 101,81,65,53 μK, which correspond to elastic s-wave collision rates of 27,23,17,14 s^{-1}, respectively. These s-wave collision rates are compatible with the points showing the temperature reduction. Parameters: $P = 200$ mW, $\Delta = 40$ GHz, $w = 65$ μm, and $f_m = 90$ kHz.

Figure 15(b) shows the cloud temperature as a function of the holding time just after compression. The cloud is compressed during 40 ms and the trap parameters are kept constant after compression. The state of the system after compression is the initial condition for this experiment: the smaller the final trap size, the denser and hotter the cloud, leading to higher s-wave collision rates. In Fig. 15(b), we notice that the temperature reduction is faster when the cloud is initially hotter and denser (i.e., the trap size after compression is smaller), which strongly hints at thermalization due to s-wave collisions. The elastic collision rates computed from Eq. (18) (see the caption of Fig. 15) are compatible with the time scale of the temperature reduction observed in Fig. 15(b). Indeed, three or four elastic collisions are needed for the gas to thermalize [35]. We note that pumping the atoms into the $F = 1$ hyperfine level (instead of $F = 2$ used in this work) would allow us to avoid unwanted hyperfine-structure-changing collisions occurring at large densities.

VI. CONCLUSION

We have studied a blue-detuned crossed dipole trap designed to quickly compress cold atomic clouds to high densities. Extensive characterization of the system has led to an understanding of the properties and the dynamics of this trapping scheme. After a very efficient loading of a large number of atoms (up to 5×10^7), the cloud is compressed in 5 ms from an initial density of 5×10^{10} cm^{-3} to a final density of 10^{13} cm^{-3}. The cloud density in the final stage is very

close to the Ioffe-Regel criterion, demonstrating the efficiency and reliability of this technique for studying light-matter interactions in the dense regime.

Extension of this work includes improving the trap performances by optimizing the trap loading (e.g., denser dark MOT, compensating for gravity, etc.), having a better control of the final compression state, or using Sisyphus cooling during the early compression stages. In addition to these modifications concerning the experimental protocol, improvements of the setup itself would lead to substantial performance leaps; using, e.g., a more detuned and powerful laser to reduce spontaneous emission losses or using VCOs with a higher input modulation bandwidth and a better frequency stability.

Increasing the trap lifetime would allow use of this setup for producing quantum-degenerate gases. This kind of compressible dipole trap would make the loading and evaporation proceed differently from the standard approach to optical BECs, yielding larger BECs more quickly. It would consist in reaching a high collision rate during a first compression stage and then realizing runaway evaporative cooling. To do so, the trap frequency should be maintained constant by reducing the trap size when the trap power is reduced. This technique would not require mobile lenses [23,36], allowing for faster and more stable operations.

ACKNOWLEDGMENTS

This work was supported by Grants No. ANR-06-BLAN-0096 CAROL and No. ANR-09-JCJC-009401 INTERLOP. We acknowledge fruitful discussions with the cold-atom group at INLN. We thank Jean-François Schaff for discussions and the imaging program.

[1] M. D. Barrett, J. A. Sauer, and M. S. Chapman, Phys. Rev. Lett. **87**, 010404 (2001).
[2] M. Greiner, O. Mandel, T. Esslinger, T. W. Hansch, and I. Bloch, Nature (London) **415**, 39 (2002).
[3] Z. Hadzibabic, P. Kruger, M. Cheneau, B. Battelier, and J. Dalibard, Nature (London) **441**, 1118 (2006).
[4] E. Akkermans, A. Gero, and R. Kaiser, Phys. Rev. Lett. **101**, 103602 (2008).
[5] R. Kaiser, J. Mod. Opt. **56**, 2082 (2009).
[6] I. M. Sokolov, M. D. Kupriyanova, D. V. Kupriyanov, and M. D. Havey, Phys. Rev. A **79**, 053405 (2009).
[7] M. O. Scully, E. S. Fry, C. H. R. Ooi, and K. Wódkiewicz, Phys. Rev. Lett. **96**, 010501 (2006).
[8] T. Bienaimé, S. Bux, E. Lucioni, P. W. Courteille, N. Piovella, and R. Kaiser, Phys. Rev. Lett. **104**, 183602 (2010).
[9] T. Bienaimé, N. Piovella, and R. Kaiser, Phys. Rev. Lett. **108**, 123602 (2012).
[10] M. O. Scully, Phys. Rev. Lett. **102**, 143601 (2009).
[11] G. Labeyrie, F. de Tomasi, J.-C. Bernard, C. A. Müller, C. Miniatura, and R. Kaiser, Phys. Rev. Lett. **83**, 5266 (1999).
[12] P. W. Anderson, Phys. Rev. **109**, 1492 (1958).
[13] A. F. Ioffe and A. R. Regel, Prog. Semicond. **4**, 237 (1960).
[14] S. R. Granade, M. E. Gehm, K. M. O'Hara, and J. E. Thomas, Phys. Rev. Lett. **88**, 120405 (2002).
[15] S. Balik, M. D. Havey, I. M. Sokolov, and D. V. Kupriyanov, Phys. Rev. A **79**, 033418 (2009).
[16] R. Grimm, M. Weidemuller, and Y. B. Ovchinnikov, Adv. At. Mol. Opt. Phys. **42**, 95 (1999).
[17] N. Friedman, L. Khaykovich, R. Ozeri, and N. Davidson, Phys. Rev. A **61**, 031403 (2000).
[18] V. Milner, J. L. Hanssen, W. C. Campbell, and M. G. Raizen, Phys. Rev. Lett. **86**, 1514 (2001).
[19] N. Friedman, A. Kaplan, D. Carasso, and N. Davidson, Phys. Rev. Lett. **86**, 1518 (2001).
[20] A. Kaplan, N. Friedman, M. Andersen, and N. Davidson, Phys. Rev. Lett. **87**, 274101 (2001).
[21] K. Henderson, C. Ryu, C. MacCormick, and M. G. Boshier, New J. Phys. **11**, 043030 (2009).
[22] B. Zimmermann, T. Müller, J. Meineke, T. Esslinger, and H. Moritz, New J. Phys. **13**, 043007 (2011).
[23] T. Kinoshita, T. Wenger, and D. S. Weiss, Phys. Rev. A **71**, 011602 (2005).
[24] A. Gozzini, F. Mango, J. Xu, G. Alzetta, F. Maccarrone, and R. Bernheim, Nuovo Cimento D **15**, 709 (1993).
[25] B. P. Anderson and M. A. Kasevich, Phys. Rev. A **63**, 023404 (2001).
[26] T. Chanelière, L. He, R. Kaiser, and D. Wilkowski, Eur. Phys. J. D **46**, 507 (2008).
[27] T. Arpornthip, C. A. Sackett, and K. J. Hughes, Phys. Rev. A **85**, 033420 (2012).
[28] J. E. Bjorkholm, Phys. Rev. A **38**, 1599 (1988).
[29] S. Bali, K. M. O'Hara, M. E. Gehm, S. R. Granade, and J. E. Thomas, Phys. Rev. A **60**, R29 (1999).
[30] M. Hammes, D. Rychtarik, and R. Grimm, C. R. Acad. Sci., Ser. IV–Phys. **2**, 625 (2001).
[31] R. Dumke, M. Volk, T. Müther, F. B. J. Buchkremer, G. Birkl, and W. Ertmer, Phys. Rev. Lett. **89**, 097903 (2002).
[32] H. Lignier, J. Chabé, D. Delande, J. C. Garreau, and P. Szriftgiser, Phys. Rev. Lett. **95**, 234101 (2005).
[33] P. W. H. Pinkse, A. Mosk, M. Weidemüller, M. W. Reynolds, T. W. Hijmans, and J. T. M. Walraven, Phys. Rev. Lett. **78**, 990 (1997).
[34] D. M. Stamper-Kurn, H.-J. Miesner, A. P. Chikkatur, S. Inouye, J. Stenger, and W. Ketterle, Phys. Rev. Lett. **81**, 2194 (1998).
[35] W. Ketterle and N. J. Van Druten, Adv. At. Mol. Opt. Phys. **37**, 181 (1996).
[36] T. Bienaimé, Ph.D. thesis, Université de Nice Sophia Antipolis, 2011.